VOL. 17, NO. 1, JANUARY 2022 ISSN 1819-6608
ARPN Journal of Engineering and Applied Sciences
©2006-2022 Asian Research Publishing Network (ARPN). All rights reserved.
www.arpnjournals.com

FLOW TOPOLOGY AROUND LOW REYNOLDS NUMBER EPPLER AIRFOILS WITH VORTEX SHEDDING

Che Intan Hartini Che Ibrahim, Aslam Abdullah and Mohd. Azahari Razali
Faculty of Mechanical and Manufacturing Engineering, Universiti Tun Hussein Onn Malaysia, Parit Raja, Batu Pahat, Johor, Malaysia
E-Mail: aslam@uthm.edu.my

ABSTRACT

The flow topology has been widely discussed over the years and serves as motivation for the process of vortex formation and the periodic behaviour of the reattachment profile research studies. This study takes three low Reynolds number Eppler airfoils into account. The computational fluid dynamics simulations carried out involve the air flow passing these models. The attention is given mainly on the separation bubble, vortex shedding and reattachment point. The corresponding effects on airfoils aerodynamic performance is observed. The method is validated against an established data to indicate that both simulations and analysis technique are reliable. The results are useful in micro aerial vehicles application where the airfoils are those of low Reynolds number.

Keywords: flow topology, vortex shedding, separation bubble, reattachment point.

1. INTRODUCTION

Flow topology concerns the structures within the flow field [1, 3]. Singular fixed points are used in analysing flow topology in order to understand the physics of flow and its complex structure (e.g. separation bubble, shedding of vortices). The construction of mathematical model in diagnosing the critical air loads can be analysed by obtaining the information of topologic bifurcation via flow topology [2, 4]. Flow topology therefore important if we are to perform deeper insight of, for instance, available analysis of flow past airfoils [5, 6], and even more specific problems involving the ground effects [7, 8].

The occurrence of vortex shedding happens when oscillating flow has once developed, grow and move before it is able to detach from the surface of the airfoil at the trailing edge. The formation and shedding of the vortices, and the encased bubble between the point of separation and reattachment point on the surface of the airfoil (i.e. separation bubble) significantly affect the aerodynamic performance of airfoils [9]. Failure of the separated flow to reattach to the surface of airfoil will lead to stall condition or loss of lift.

At low Reynolds number regime, the formation of separation bubble on the surface of airfoil can be longer until it reaches complete flow separation leading to stall condition [10]. Hence, the design and geometry of low Reynolds number airfoils can reduce the risk of the complete separation in the application of, for instance, micro aerial vehicle (MAV).

The study considers three low Reynolds number airfoils from series of Eppler (i.e. E387, E392, E374). It highlights the formation and development of separation bubble and vortex shedding, and their relations to the lift coefficient of the airfoils by using the method of singular fixed point.

The study aims at the formation of vortex shedding and separation bubble effects on the airfoils' aerodynamic performance.

2. LOW REYNOLDS NUMBER AIRFOILS

The geometry of the low Reynolds number airfoils are shown in Figure-1. Respective grid, computational domain and boundary conditions are shown in Figure-2.

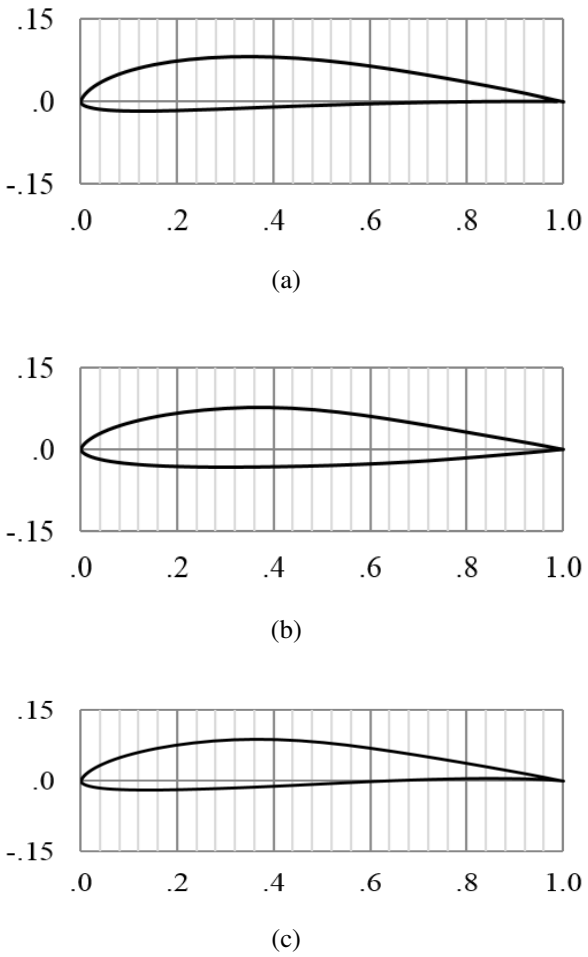

Figure-1. Geometry of low Reynolds number airfoils (a) E387 (b) E374 (c) E392.

©2006-2022 Asian Research Publishing Network (ARPN). All rights reserved.

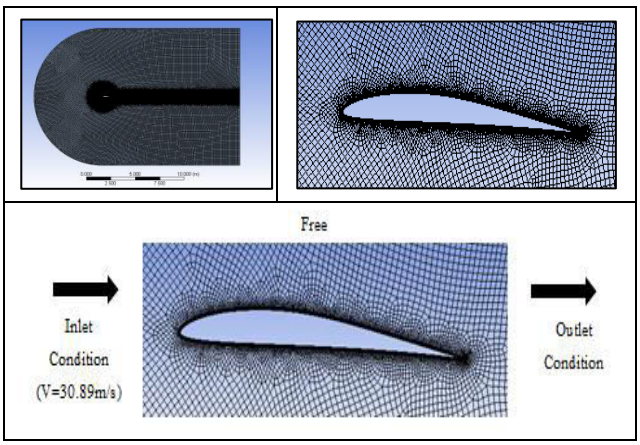

Figure-2. Grid, domain and boundary conditions.

3. TOPOLOGICAL OVERVIEW

In this study, both vortex shedding and separation bubble profile information are gained by means of the topological overview of the flow. The model of laminar has been proven in yielding better result for observing flow topology with vortex shedding [4, 11]. The flow development involves the velocity curl profile over the airfoils in fixed laminar condition, with respect to time. In this simulation, two-dimensional flows over a set of airfoils (i.e. Eppler) are examined. The free stream velocity is 30.89 ms^{-1} and the Reynolds number is Re = 60 000. These wing types are applicable for MAVs and Re = 60 000 is in the typical range of MAV operation [2]. The chord length of each airfoil is set as 1 meter. A time step of t = 0.0015 unit time is used for accuracy, but to conserve memory only every 8th timestep is stored. Therefore, the time step for the exported data files is t = 0.012 time units. In this simulation, 600 velocity time steps were analyzed, for $\alpha = 4^{\circ}$. The Cartesian mesh covers the domain $-7 \text{ m} \le x \le 14 \text{ m}$, $-7 \text{ m} \le y \le 7 \text{ m}$, with the initial grid spacing of $\Delta x = \Delta y = 0.02$ m. This grid spacing is necessary to capture the fine detailed structures in the wake region and to ensure the accuracy of the manifold calculations. The accurate calculation of Lagrangian coherent structures requires that the grid spacing be small [2]. The transition time is set to $\Delta t = 0.012$ unit time to optimize the appearance of the desired flow structures. Longer transition times lead to the lost of important features while shorter transition times fail to reveal the desired level of detail.

All the airfoils are simulated at 4^{o} angle of attack and Reynolds number of 60,000 with a commercial CFD software. In general 'proximity and curvature' size function, fine relevence center, and maximum face size of 0.1 m are chosen. Type of body sizing is '(two) body of influence' with element and size growth rate of 0.02 m and 1.2, respectively, and '1 body' geometry selection. 'Edge sizing 1' type is 'number of (250) divisions', with sizing behaviour and the geometry are set to be hard and consists of 2 edges, respectively. Edge sizing 2 type is also 'number of (5) divisions', with sizing behaviour is set to be hard for '1 edge' geometry. The selected options for inflation technique are '1 face' geometry, '3 edges' boundary, and inflation of 'total thickness' type with 10 layers, 1.2 growth rate, and 0.01 m maximum thickness.

In general the setup includes density based solver, absolute velocity formulation, transient condition and planar 2D space. Laminar model is used, while energy equation model is not considered. Constant air density and viscosity values are 1.225 kg/m^3 and 1.7894 x 10^{-05} kg/m.s, respectively. Boundary conditions include no slip wall condition, inlet velocity, 'magnitude and direction' velocity specification method, absolute reference frame, zero initial gauge pressure, and component x-y = (1,0) of flow direction. Outlet type is that of 'pressure-outlet', where absolute backflow reference frame, zero pressure gauge, and 'normal to boundary' backflow direction specification method, are employed. The solution method is that of implicit, with Roe Flux-Difference Splitting scheme, spatial discretization of least squares cell based and second order upwind for estimating spatial gradient and flow, respectively. The transient formulation is that of second order implicit. In the solution initialization process, we set standard initialization method which computes from inlet, with the reference frame that is relative to cell zone, initial non-zero velocity value only as x-component, and initial zero gauge pressure.

The calculation activities are autosaved every 8 time steps. Fixed time stepping method is applied, with 600 number of time steps, the maximum of 3700 iterations per reporting interval, and a single profile update interval.

4. FLOW TOPOLOGY AROUND E387

In E387 case, the reverse saddle-node bifurcation and shedding of vortex occur at t_1 and t_2, respectively. Figure-3 shows the flow topology of airfoil E387 at three different times. The dash lines on the figure indicate the segment boundaries. All fixed point location at three different times have been validated by Hunt relationship. Table-1 shows the Hunt relationship based finding summary.

©2006-2022 Asian Research Publishing Network (ARPN). All rights reserved.

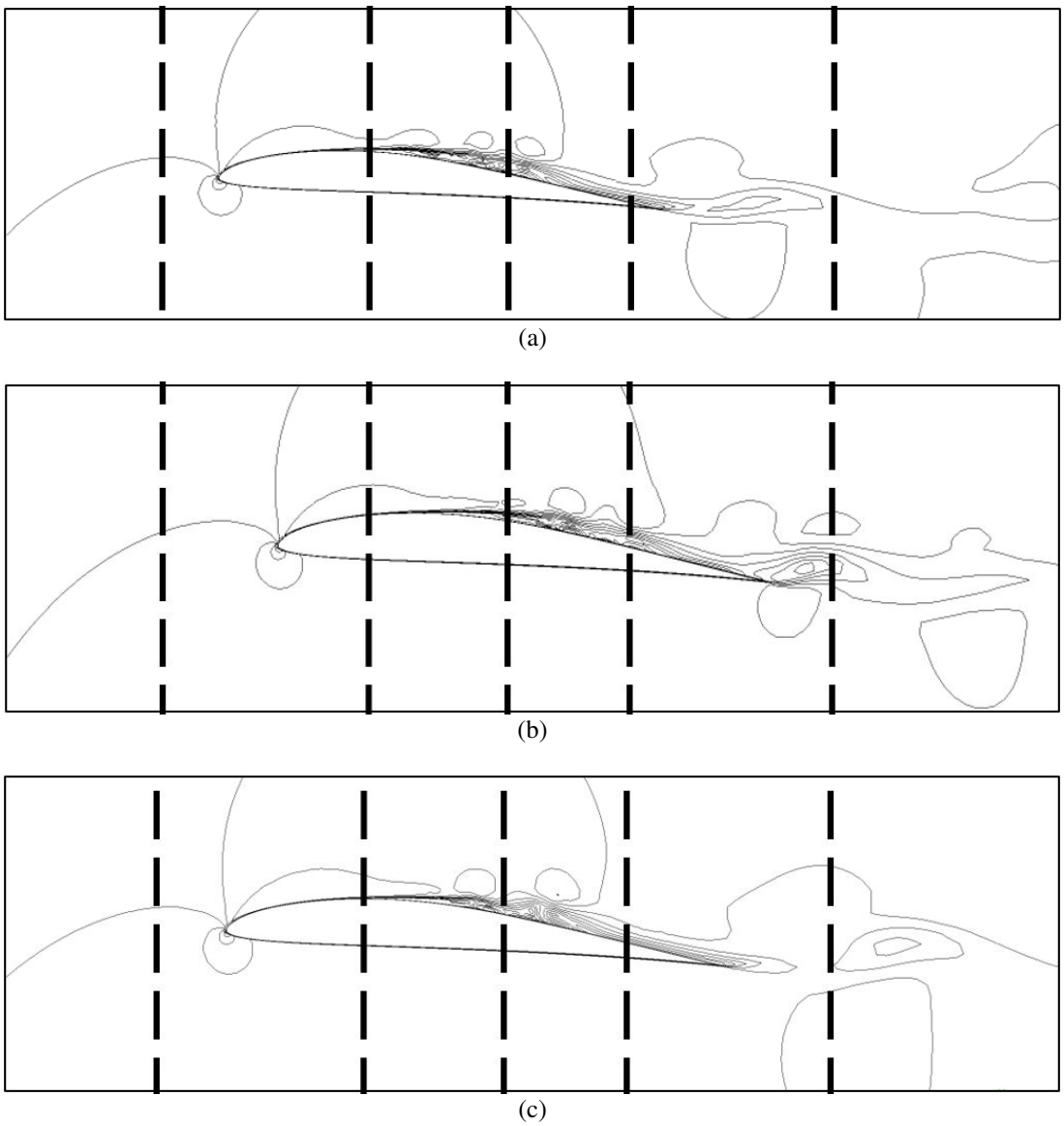

Figure-3. Flow topology around E387 with Re = 60,000 at $\alpha = 4^{o}$ at time (a) t_1 (b) t_2 (c) t_3.

Table-1. Summary of topological fixed points in the flow over Eppler E387.

Segment	Four-Way Elliptic Fixed Points (E)	Three-Way Elliptic Fixed Points (E')	Four-Way Hyperbolic Fixed Points (H)	Three-Way Hyperbolic Fixed Points (H')
t_1	12	0	9	8
t_2	11	0	7	10
t_3	10	0	6	10

In segment 1, there is no occurrence or movement of fixed points on the surface of the airfoil. The hyperbolic fixed point on the surface of the airfoil (i.e. that in the middle of the section) is the initiating point of the separation bubble.

In segment 2, the occurrence of separation bubble is observed. At t_1, the hyperbolic fixed points, H1 and H2 collide each other to form new hyperbolic fixed point just below an elliptic fixed point, E1. Consequently, the new point collides with E1. The collision between these two fixed points is called reverse-saddle node bifurcation. Reverse-saddle node bifurcation causes the collided points to cancel out each other which enable new vortex to separate from the separation bubble towards the trailing edge of the airfoil.

At t_2 in segment 2, the separation bubble becomes smaller, resulting from the occurrence of reverse-saddle node bifurcation that separates a new vortex from the bubble (see Figure-4).

©2006-2022 Asian Research Publishing Network (ARPN). All rights reserved.

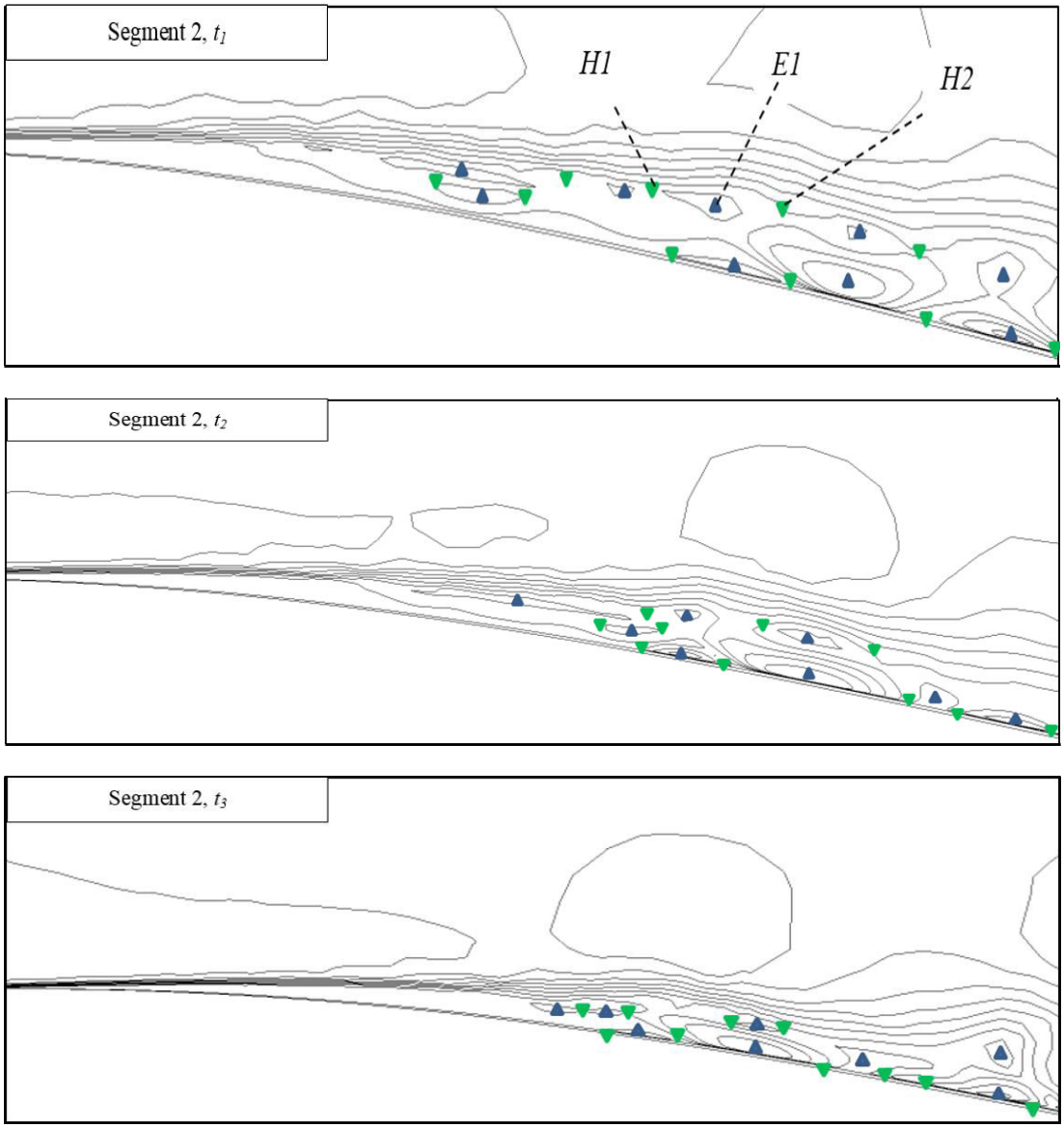

Figure-4. Segmented flow topology (segment 2) around E387 with Re = 60,000 at $\alpha = 4^o$.

Observation on segment 3 indicates that there is no occurrence involving the issue of interests at three different times. Although changes in flow topology pattern are observables, no further process is seen (see Figure-5). The hyperbolic fixed point labelled as H3 at t_2 will be further discussed in segment 4.

©2006-2022 Asian Research Publishing Network (ARPN). All rights reserved.

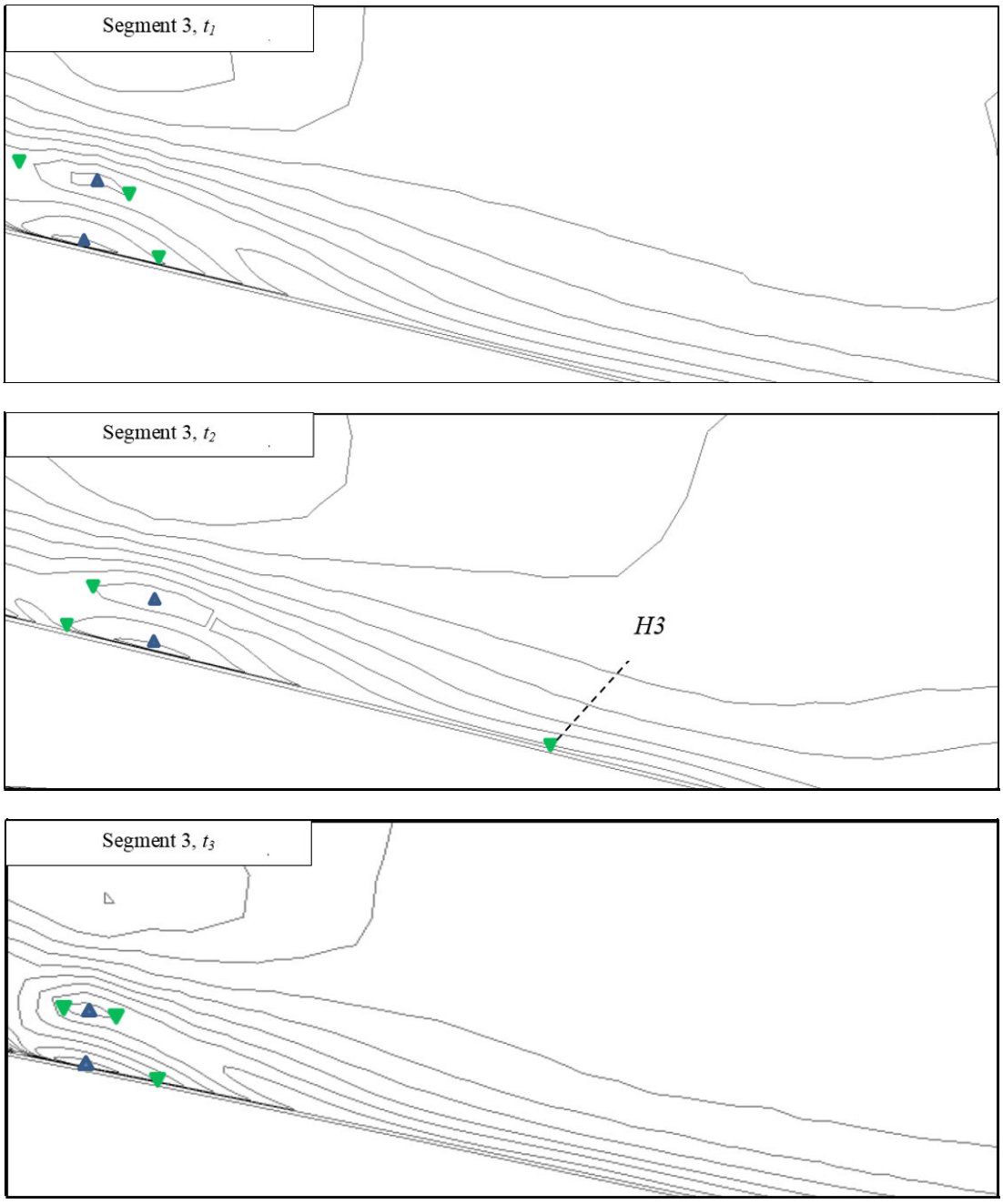

Figure-5. Segmented flow topology (segment 3) around E387 with Re = 60,000 at $\alpha = 4^o$.

A hyperbolic fixed point, H4 in segment 4 collides with another point, H3 in segment 3. The collision causes the corresponding vortex to be completely separated from the surface of the airfoil which can be observed at t_3. This initiates the occurrence of vortex shedding. The resulting newly formed hyperbolic fixed point is located just below the shed vortices (see Figure-6).

©2006-2022 Asian Research Publishing Network (ARPN). All rights reserved.

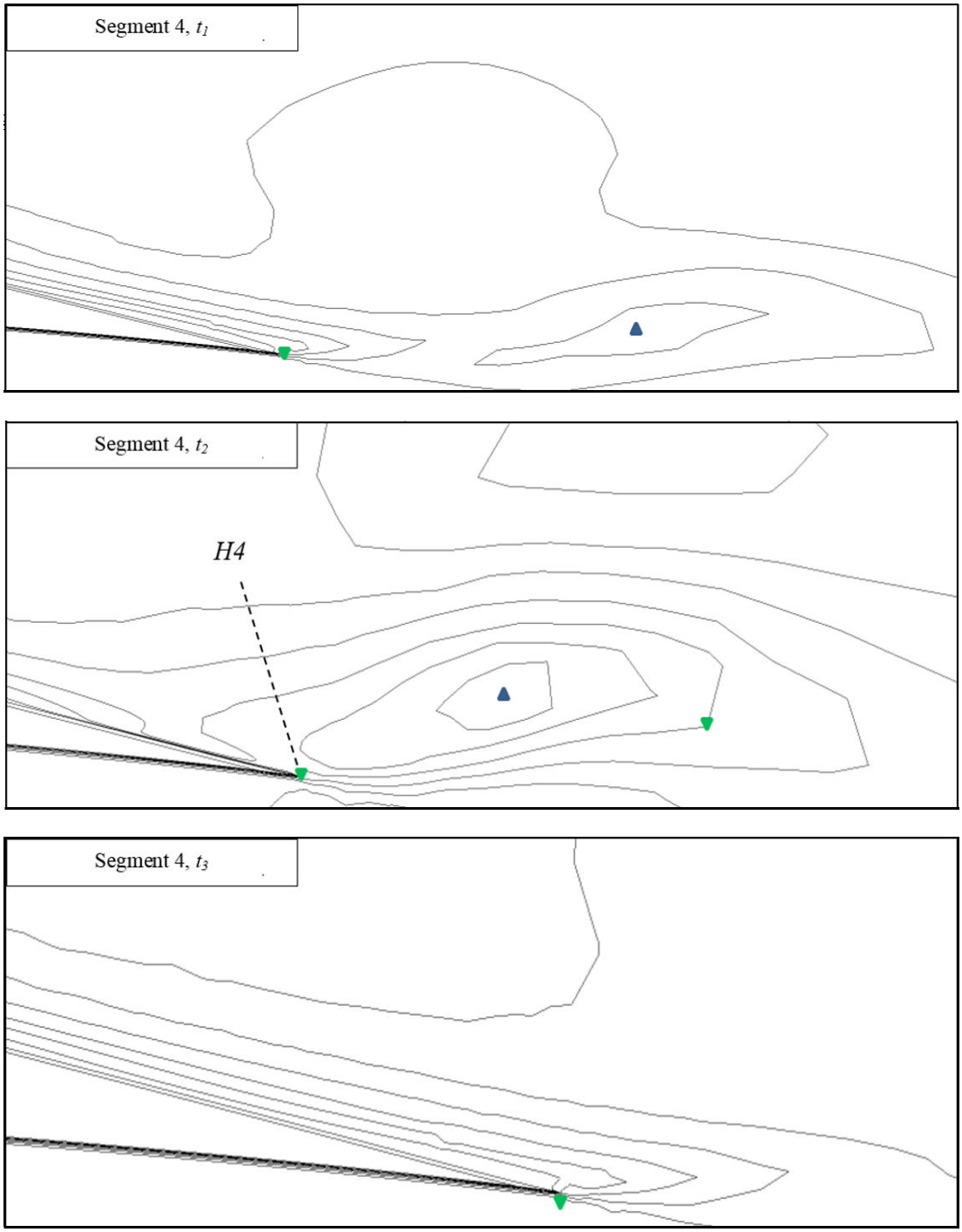

Figure-6. Segmented flow topology (segment 4) around E387 with Re = 60,000 at $\alpha = 4^o$.

The downstream of the airfoil is illustrated in segment 5 in which the shed vortices appear. Note, however, that any occurrence in this segment is beyond the scope of this work.

The values in Table-1 are substituted in equation:

$$\left(\sum E + \tfrac{1}{2}\sum E'\right) - \left(\sum H + \tfrac{1}{2}\sum H'\right) = 1 - n \quad (1)$$

where $n = 2$.

Table-2. Values of c_l and c_d.

Time	c_l	c_d
t_1	8.0847×10^{-1}	2.9893×10^{-2}
t_2	7.1044×10^{-1}	1.5254×10^{-2}
t_3	7.8078×10^{-1}	2.2039×10^{-2}

Flow topology at t_1 shows the thinner separation bubble which makes the air flow smoother on the surface of the airfoil. At t_1 also, reverse saddle-node bifurcation

©2006-2022 Asian Research Publishing Network (ARPN). All rights reserved.

occurs which resulting from the collision of E1 with the newly formed hyperbolic fixed point due to the collision between H1 and H2. The occurrence of vortex shedding is not observed at the trailing edge of the airfoil. Hence, the airfoil does not experience the effects of vortex shedding at this stage/time. From these multiple occurrences, the value of lift coefficient at t_2 is the highest among those at three different times.

At t_2, the vortex at the trailing edge of the airfoil is by now ready to shed. The shedding would take place once H3 and H4 collide which causes the formation of a new hyperbolic fixed point below the shed vortex. Due to the occurrences of vortex shedding, the value of lift coefficient was the lowest at t_2.

At t_3 which is the time just after the vortex is completely shed and detached from the surface, the lift coefficient is slightly higher than that at t_2.

5. FLOW TOPOLOGY AROUND E374

The reverse saddle-node bifurcation occurs in E374 case at t_1 while shedding of vortex occurs twice at t_2 and t_3. The agreement between the topology and the corresponding Hunt relationship is given in Table-3.

In segment 1, there is no occurrence at the three different times, while in segment 2, reverse saddle node bifurcation occurs at t_1 which involves the collision between an elliptic fixed point, E1 and a hyperbolic fixed point, H1. The collision splits the existing vortex into two vortices on the surface of the airfoil. The flow topology in segment 2 is shown in Figure-7.

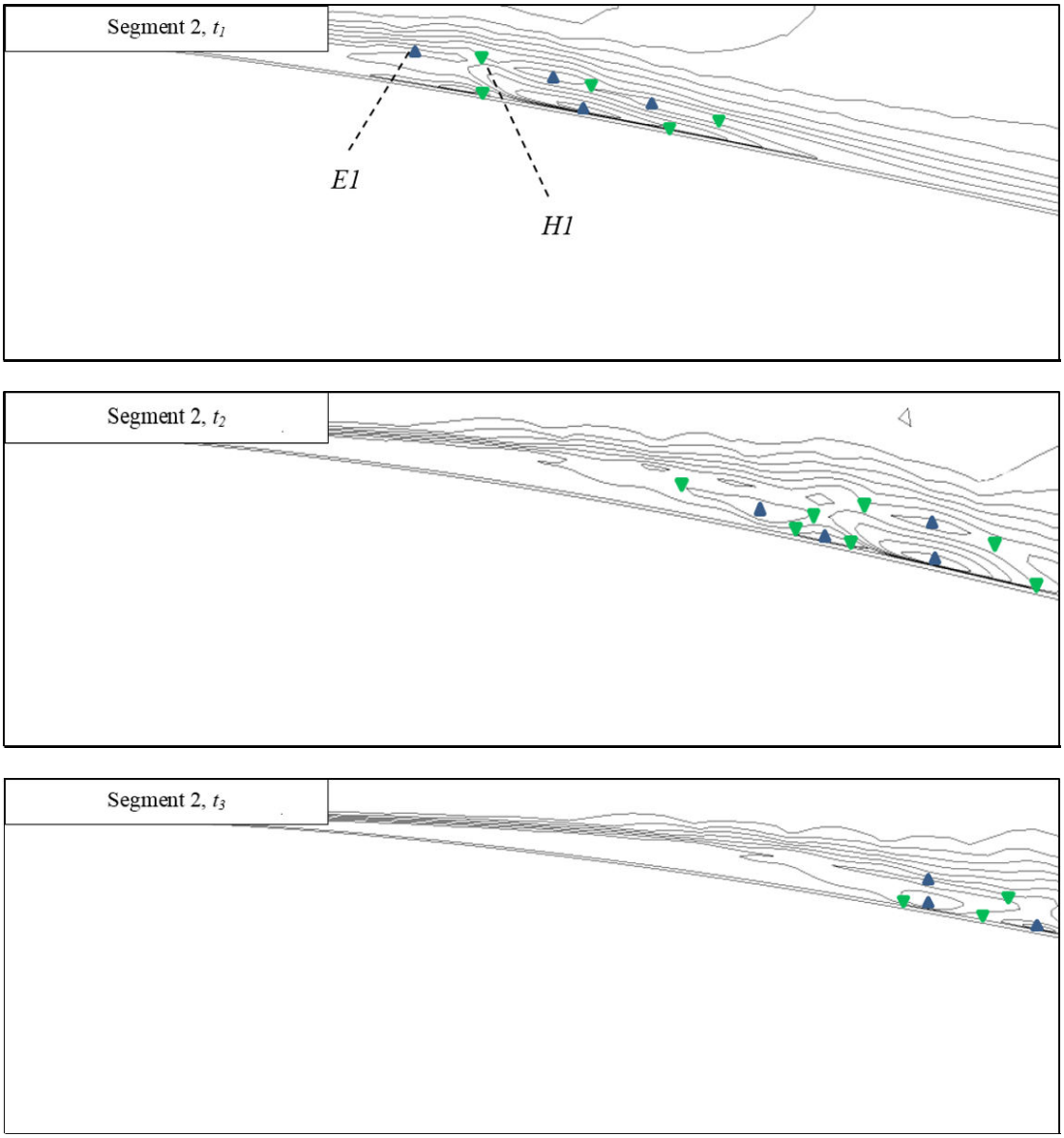

Figure-7. Segmented flow topology (segment 2) around E374 with Re = 60,000 at α = 4°.

©2006-2022 Asian Research Publishing Network (ARPN). All rights reserved.

Table-3. Summary of topological fixed points in the flow over Eppler E374.

Segment	Four-Way Elliptic Fixed Points (E)	Three-Way Elliptic Fixed Points (E')	Four-Way Hyperbolic Fixed Points (H)	Three-Way Hyperbolic Fixed Points (H')
t_1	5	0	4	6
t_2	10	0	7	10
t_3	8	0	5	10

In segment 3, there is no occurrence of interest. However, the transition and the movement of vortices can be seen.

The event of vortex shedding can be observed twice in segment 4 which is at t_2 and t_3 due to the collisions of H3-H4, and H5-H6, respectively (see Figure-8). Segment 5 corresponds to the downstream of the airfoil in which the shed vortices appear.

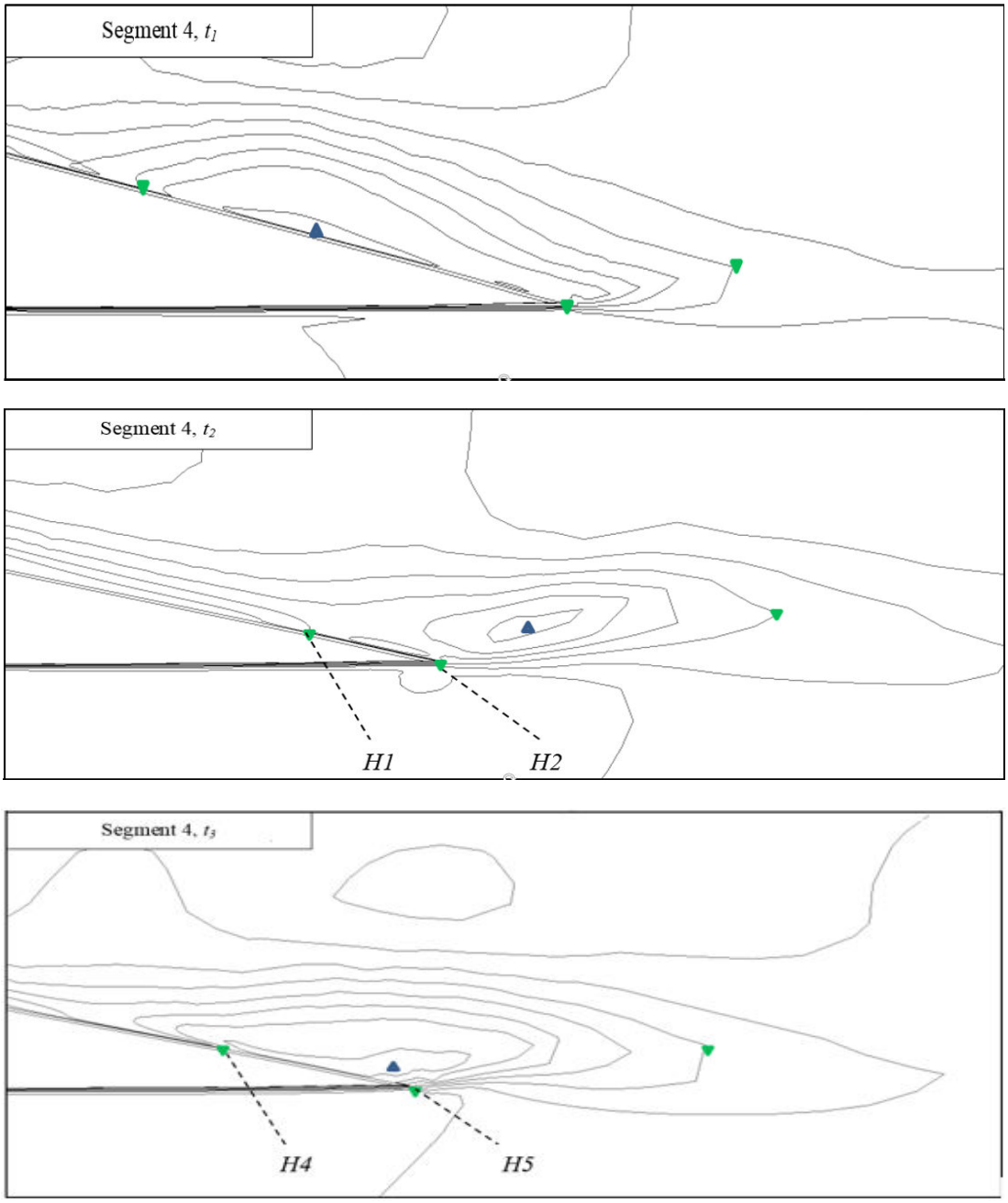

Figure-8. Segmented flow topology (segment 4) around E374 with Re = 60,000 at α = 4°.

©2006-2022 Asian Research Publishing Network (ARPN). All rights reserved.

Substituting the values in Table 3 into (1), we have $n = 3$.

Table-4. Values of c_l and c_d.

Time	c_l	c_d
t_1	5.6640×10^{-1}	1.8709×10^{-2}
t_2	5.0579×10^{-1}	1.2383×10^{-2}
t_3	4.4867×10^{-1}	4.8104×10^{-3}

The highest lift coefficient of 5.6640×10^{-1} is observed at t_1, while the lowest coefficient of 4.4867×10^{-1} is found at t_3.

From the topological overview, the thickness of the separation bubble affects the drag. At t_3, the drag is the lowest since the bubble is at its minimum thickness. However, the lift decreases at the same time (i.e. at t_3) due to the presence of vortex shedding.

6. FLOW TOPOLOGY AROUND E392

At t_1 in E392 case, the reverse saddle-node bifurcation takes place, while at t_3 the vortex is shed. In Table-5, the summary of topological fixed points is shown.

There is no interested event in segment 1. However, reverse saddle node bifurcation takes place in segment 2 at t_1 after an elliptic fixed point, E1 collides with a newly formed hyperbolic fixed point (i.e. that results from the collision of H1 and H2). The collision separates a newly formed vortex from the existing one. The segmented flow topology in segment 2 is illustrated in Figure-9.

Table-5. Summary of topological fixed points in the flow over E392.

Segment	Four-Way Elliptic Fixed Points (E)	Three-Way Elliptic Fixed Points (E')	Four-Way Hyperbolic Fixed Points (H)	Three-Way Hyperbolic Fixed Points (H')
t_1	12	0	8	10
t_2	11	0	7	10
t_3	11	0	9	6

©2006-2022 Asian Research Publishing Network (ARPN). All rights reserved.

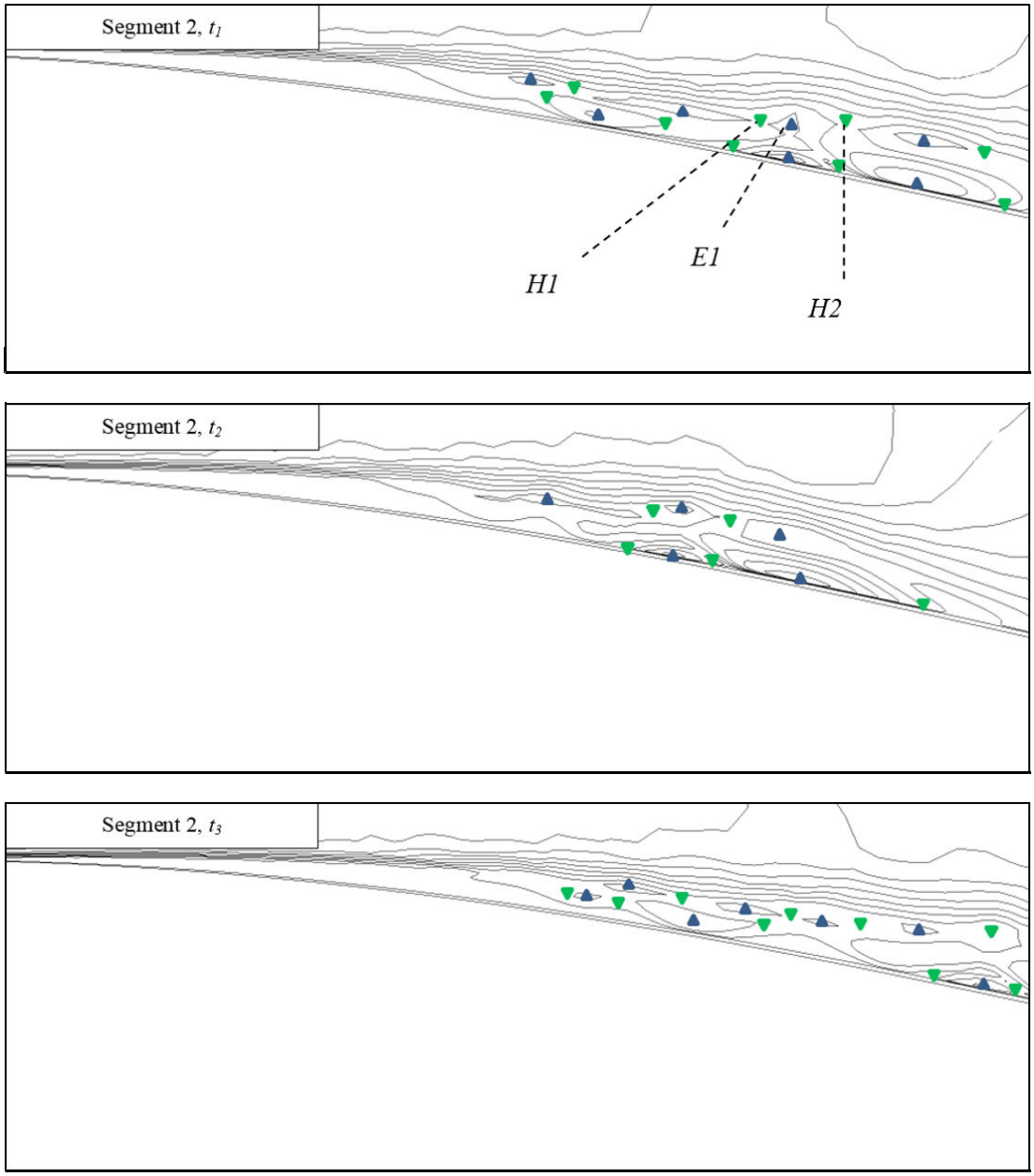

Figure-9. Segmented flow topology (segment 2) around E392 with Re = 60,000 at α = 4°.

Despite changes in flow topology pattern in segment 3, the segment shows no significant event. The hyperbolic fixed point H3 in segment 3 will involve in the collision with another hyperbolic point in segment 4, H4 at t_3 (see Figure-10 and Figure-11). This collision initiates the vortex shedding.

©2006-2022 Asian Research Publishing Network (ARPN). All rights reserved.

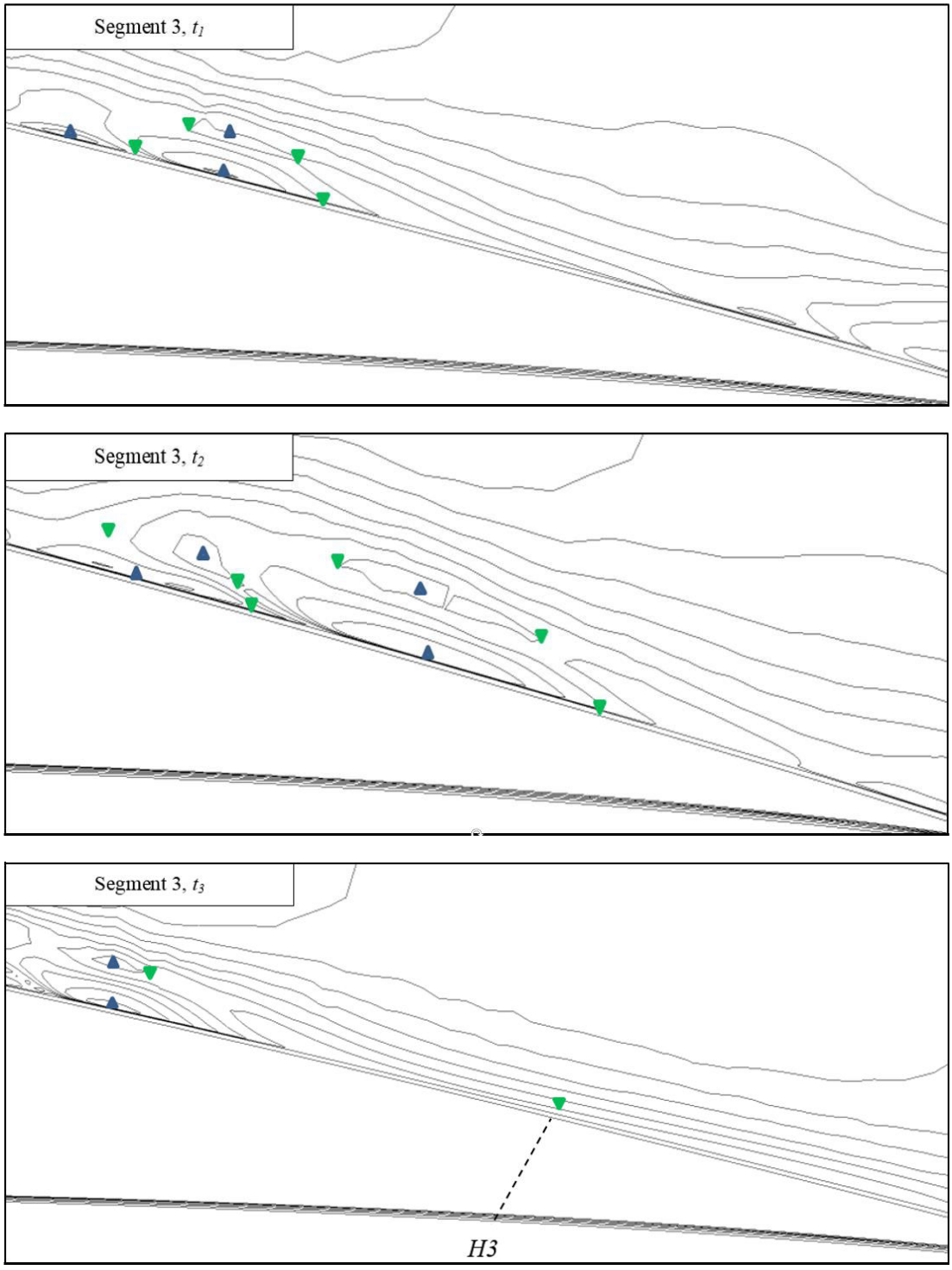

Figure-10. Segmented flow topology (segment 3) around E392 with Re = 60,000 at α = 4°.

©2006-2022 Asian Research Publishing Network (ARPN). All rights reserved.

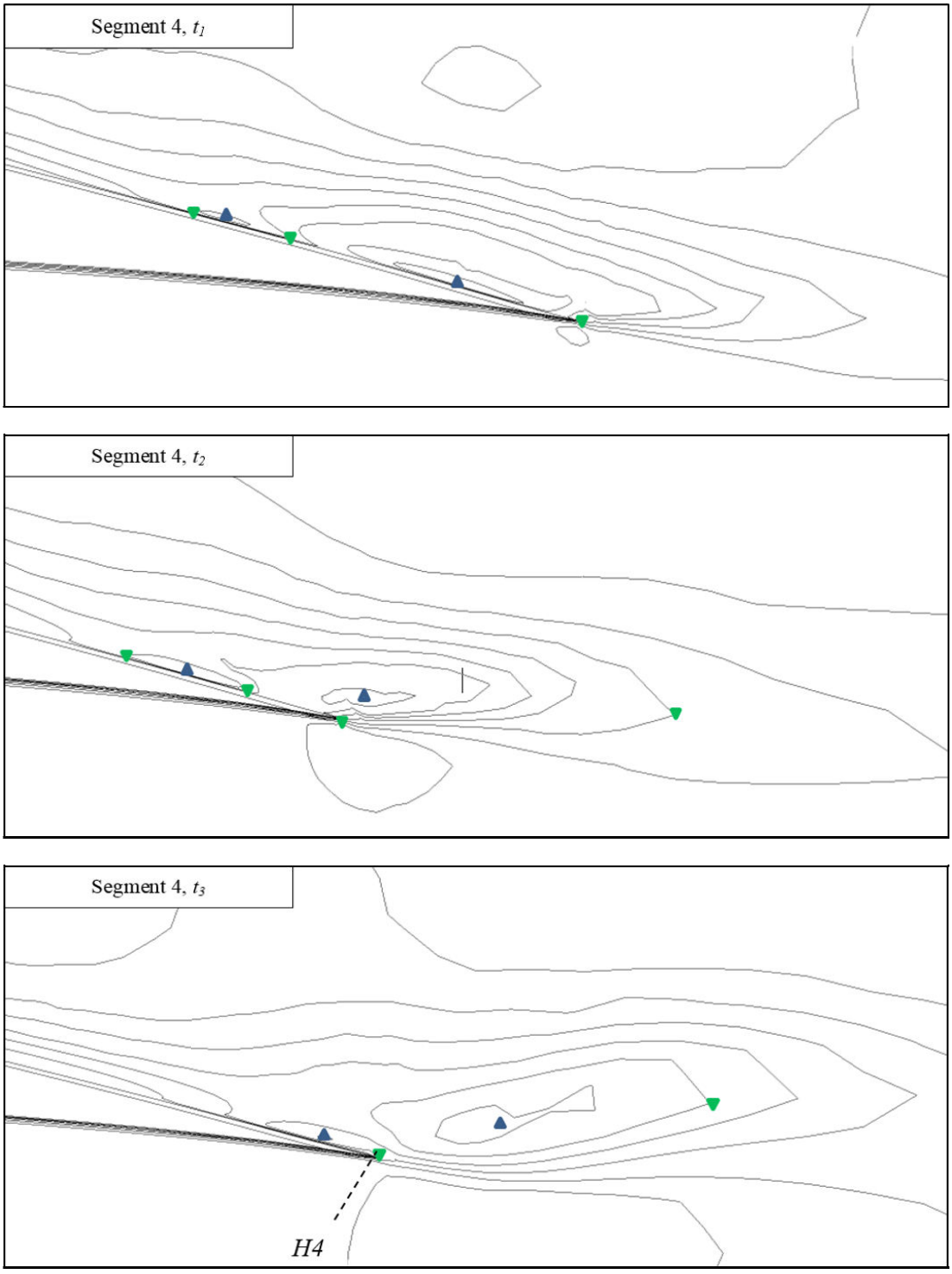

Figure-11. Segmented flow topology (segment 4) around E392 with Re = 60,000 at α = 4°.

Segment 5 highlights the area behind the airfoil and portrays the shed vortex that has been detached from the surface of the airfoil.

We have $n = 2$, after substituting the values in Table-5 into (1).

Table-6. Values of c_l and c_d.

Time	c_l	c_d
t_1	6.6406×10^{-1}	2.7324×10^{-3}
t_2	6.9714×10^{-1}	8.1822×10^{-3}
t_3	6.7221×10^{-1}	5.3508×10^{-3}

©2006-2022 Asian Research Publishing Network (ARPN). All rights reserved.

The highest lift is obtained at t_2 where the lift coefficient takes the value of 6.9714×10^{-1}. At t_1, the coefficient takes the smallest value of 6.6406×10^{-1}.

The lift at t_2 is high in comparison to that at t_1 due to the relatively shorter reattachment length (see segment 2 in Figure-11), while the presence of a secondary separation bubble at t_2 in segment 3 contributes to high drag.

Thinner vortices can be seen at t_3 which is caused by the reverse saddle-node bifurcation. Thus, the drag is lower at this time. The lift at t_3, however, decreases as a result of vortex shedding.

7. CONCLUSIONS

Based on the simulation and analysis of low Reynolds number Eppler airfoils, there are several findings which are useful in the application of micro aerial vehicle. Firstly, the design of these airfoils makes them to resist to complete flow separation which would lead to the lift drop. Typical airfoils tend to have complete flow separation when operate in low Reynolds number regime.
The separation bubble formed on the surface of the airfoil disturbs the flow of air along the surface. When the air passes the bubble, the velocity of air decreases, thus causes the rise in pressure that would lead to boundary layer separation. The boundary layer is originally in tangential direction to the surface and is highly sensitive to any disturbance as the separation bubble. If a disturbance leads to instability, then the laminar flow would become turbulence which is a state unfavourable to any flying device. In the case of low Reynolds number airfoils, the streamlines reattach to the airfoil surface while passing the separation bubble, thus prevent the transition to turbulent flow.

If a separation bubble is formed, it needs to contain as few vortices and to be as thin as possible in order to avoid complete flow separation. Thicker separation bubble which might be associated to more vortices it contains degrades the lift and increases the drag.

Finally, the vortex shedding directly lowers the lift and increasing the drag. Shedding of vortices is one of the unfavourable conditions in flying machines and cannot be totally eradicated. Nevertheless, giving the right technique, its effects can be minimized.

ACKNOWLEDGEMENT

The authors would like to thank Universiti Tun Hussein Onn Malaysia (UTHM) and Ministry of Higher Education Malaysia (MoHE) for the research facilities.

REFERENCES

[1] Moffatt H. K. 2001. Some remarks on topological fluid mechanics. An introduction to the geometry and topology of fluid flows. Springer, Dordrecht: 3-10.

[2] Lipinski D., Cardwell B. and Mohseni K. 2008. A Lagrangian analysis of a two-dimensional airfoil with vortex shedding. Journal of Physics A: Mathematical and Theoretical. 41(34): 344011.

[3] Rubenstein D., Yin W. and Frame, M. D. 2015. Biofluid mechanics: an introduction to fluid mechanics, macrocirculation, and microcirculation. Academic Press.

[4] Hadi M. I., Nazri M. and Abdullah A. 2020. Vortex formation in unsteady flow over NACA 4412 and NACA 4424 airfoils. ARPN J. Eng. Appl. Sci. 15(1): 27-33.

[5] Abdullah A., Roslan A. and Omar Z. 2018. Comparative study of turbulent incompressible flow past NACA airfoils. ARPN J. Eng. Appl. Sci. 13(21): 8527-8530.

[6] Abdullah A., Jafri M. N. S. M. and Zulkafli M. F. 2017. Numerical study of military airfoils design for compressible flow. ARPN J. Eng. Appl. Sci. 12(24): 7129-7133.

[7] Abdullah A., Yazi M. N., Ghafir M. F. A., Mohd S. and Rahim M. Z. 2017. Ground proximity effect on the flow over NACA 4412 multi-element airfoil in clean configuration. Journal of Physics: Conference Series. 914(1): 1-7.

[8] Abdullah A., Kamsani M. A. and Abdullah K. 2017. Effect of ground proximity on the flow over STOL CH750 multi-element airfoil. IOP Conference Series: Materials Science and Engineering. 243(1): 1-7.

[9] Rashidi S., Hayatdavoodi M. and Esfahani J. A. 2016. Vortex shedding suppression and wake control: A review. Ocean Engineering. 126: 57-80.

[10] Kurtulus D. F. 2011. Introduction to micro air epts, design and applications. Feedback. 3: 5.

[11] Hadi M. I., Nazri M. and Abdullah A. 2019. Study of vortex behavior in unsteady flow over NACA 0012 and NACA 0024 airfoils. ARPN J. Eng. Appl. Sci. 14(22): 3840-3846.